

10 flight time in summer and of the order of 35–40 % of the flight time in winter in the tro-
11 posphere between 350 and 190 hPa in the Northern Hemisphere, over a region ranging
12 from North America to Europe. These seasonal frequencies are very low in the lower strato-
13 sphere because of the low water content (Sanogo et al., 2024). Above 200 hPa, ISSRs
14 is more frequent in tropical deep convective regions and over the North Atlantic Ocean
15 (Spichtinger et al., 2003). In terms of size, more than 80% of ice-supersaturated path
16 lengths measured along aircraft flight routes in the North Atlantic are shorter than 10 km
17 (Reutter et al., 2020; Wolf et al., 2024). The occurrence of ISSRs is favored by partic-
18 ular meteorological conditions such as deep convection, mesoscale gravity waves (Spichtinger,
19 Gierens, & Dörnbrack, 2005), a divergent flow (Gierens & Brinkop, 2012; Krämer et al.,
20 2009; Wilhelm et al., 2022), or the moist air streams in synoptic disturbances (e.g., warm
21 conveyor belt, cold and warm fronts) (Gierens & Brinkop, 2012; Wolf, Bellouin, & Boucher,
22 2023).

23 The occurrence of an ISSR is a prerequisite for the in situ formation of natural cir-
24 rus clouds, persistent contrails and contrail-induced cirrus (Minnis et al., 2004; Krämer
25 et al., 2016; Kärcher, 2018). Natural cirrus play an important role in the energy bud-
26 get and may form in situ via homogeneous nucleation at temperatures below -38°C and
27 RH_i exceeding 140 % (Heymsfield et al., 2017; Kanji et al., 2017) or via heterogeneous
28 freezing at temperatures lower than 0°C and RH_i above 100 % in the presence of ice nu-
29 cleating particles (Heymsfield et al., 2017). For a pressure range between 325 and 175 hPa,
30 aircraft flying using the kerosene as fuel can produce contrails for 1 to 15 % of the flight
31 time in the tropics and 6 to 20 % of the flight time in the mid and high latitudes regions
32 (Sanogo et al., 2024). Contrails can persist and grow for several hours in the ISSRs (Kärcher,
33 2018). Over time, such persistent contrail cirrus can evolve into cirrus clouds and me-
34 teorological conditions such as wind shear and turbulence can extend their spatial cov-
35 erage and reduce their ice crystal concentrations (Kärcher, 2018). Contrails can thus en-
36 hance the coverage of cirrus clouds (Stubenrauch & Schumann, 2005) and together, con-
37 trails and contrail cirrus, ~~are~~ referred to as aviation-induced cloudiness (AIC), which is
38 associated with a potentially significant radiative impact (Boucher et al., 2013; Bock &
39 Burkhardt, 2016; Lee et al., 2021), at least in comparison to the CO₂ radiative forcing
40 due to aviation.

41 Reducing the climate impact of AIC, along with other environmental and climate
42 impacts, is one of the main challenges facing the aerospace industry. In this perspective,
43 both academia and the private sector are looking into how aircraft trajectories can be
44 optimized to minimise fuel consumption (and the associated CO₂ emissions) while avoid-
45 ing regions favorable to the formation of contrails. This strategy requires accurate fore-
46 casts of ISSRs but also a better understanding of the physical mechanisms involved in
47 the formation and dissipation of contrails and induced cirrus (Kärcher, 2018).

48 Climate models are essential for studying contrails and their radiative effects. How-
49 ever, the formation of ISSRs and contrails occurs at scales smaller than the grid size of
50 these models, requiring the parameterization of the small scale processes. In the LMDZ
51 model, the ISSR formation processes are parameterized using a statistical treatment of
52 sublimation and condensation based on the total water distribution, as detailed in Sec-
53 tion 2.1. It is known that parameterizations are a significant source of uncertainty in cli-
54 mate models (Hourdin et al., 2017). For instance, a study by Perini et al. (2023) have
55 shown that the radiative effects of AIC are sensitive to the values of free parameters in
56 the climate model (e.g., those that control the contrail lifetime), underscoring the fact
57 that many of these parameters do not have a unique value. To reduce these uncertain-
58 ties, machine learning methods are more and more used to tune and rigorously select the
59 best value of the free parameters for a given physical process under observational con-
60 straints (Jebeile et al., 2023). For example, D. Williamson et al. (2015) used a tuning
61 method based on History Matching and iterative refocusing (see Section 3.1) to explore
62 the parametric uncertainties associated with the global mean temperature and salinity

63 Si je me trompe pas l'approche est de Vernon, Goldstein, & Bower, 2010 et de Williamson et al., 2013 (qui a notamment ajouté
64 les emulateurs à la méthode proposé par Vernon 2010). Fred que tu cites après est plus utilisateur de la méthode pour les
65 modèles de climat. Alors que Daniel Williamson fait vraiment toute la recherche qu'il y a dans l'aspect mathématiques de la
66 méthodes. Je pense que c'est bien que cette différence se sente dans ton introduction ; qu'ils ne soient pas mis au même
67 niveau.

Si tout ce paragraphe concerne la zone stratosphère par opposition à ce qui est dit
au dessus, je saigère un changement de paragraphe ou/et de changer "are very low" en
"are much lower".

together

Je ne
peux
pas signer
un papier
qui écrit
ce
est quoi les chiffres
Pour moi: insister
sur l'impact d'altitude
sur l'augmentation de modèle
Km

123 in the NEMO (Nucleus for European Modelling of the Ocean) ocean model. Similarly,
 124 Hourdin et al. (2021) applied the same approach to LMDZ, identifying model configu-
 125 rations that were more consistent with observations than the manually fine-tuned base
 126 configuration. The use of this method can also avoid the underestimation of uncertainty
 127 in climate change projections (Hourdin et al., 2023). In this study, we apply this approach
 128 of D. Williamson et al. (2015); Hourdin et al. (2021, 2023) to investigate errors in the
 129 atmospheric component (LMDZ) of the IPSL climate model, focusing on the spatial and
 130 temporal distributions of ice-supersaturated regions (ISSRs). Furthermore, we aim to
 131 identify LMDZ configurations that not only match observed ISSR properties but also
 132 align with observations of high-level cloud fractions and radiative fluxes, to ensure that
 133 the model's performance on other critical properties, such as the radiation budget, is pre-
 134 served.

135 This manuscript is structured as follows. Section 2 describes LMDZ and its param-
 136 eterizations of ISS and cloud. Section 3 details the experimental setup and our tuning
 137 approach while Section 4 presents our results. Finally, Section 5 summarizes our main
 138 findings.

139 2 LMDZ and its parameterizations of cloud

140 LMDZ is the atmospheric component of the Institute Pierre-Simon Laplace climate
 141 model known as IPSL-CM which is used for understanding the climate system and its
 142 response to various perturbations. The version used in this study is LMDZ6A, noted LMDZ
 143 in the following for the sake of simplicity, and described in details in Hourdin et al. (2020),
 144 Boucher et al. (2020) and Lurton et al. (2020). Its dynamical core is based on a mixed
 145 finite difference/finite volume discretization of the primitive equations of meteorology
 146 and transport equations and is coupled to a set of physical parameterizations (Hourdin
 147 et al., 2013).

148 The parameterization of clouds in LMDZ is based on the representation of sub-grid
 149 total water (q) using a probability density function (PDF, noted $P(q)$), whose variance
 150 and skewness, towards large humidity values increase when convective plumes bring hu-
 151 mid air from the surface to the drier free and upper tropospheres (Hourdin et al., 2020;
 152 Madeleine et al., 2020). For convective and high-level clouds (i.e., at altitude typically
 153 above ~ 6.5 km), $P(q)$ of the specific humidity is a generalized log-normal distribution
 154 (Bony & Emanuel, 2001; Madeleine et al., 2020). It is determined by its first and sec-
 155 ond moments, defined here as the mean (q_t) and the standard deviation $\sigma = \xi(p) q_t$
 156 of the gridbox total water distribution, respectively. The function $\xi(p)$ is used to impose
 157 a variation of σ as a function of pressure p . The function $\xi(p)$ increases as pressure de-
 158 creases to reach an asymptotic value of ξ_{300} at 300 hPa and in the upper troposphere.
 159 This parameter has been used as a tuning coefficient (Madeleine et al., 2020). The gridbox-
 160 averaged total humidity value q_t is related to $P(q)$ through the following equation:

$$q_t = \int_0^{+\infty} q P(q) dq$$

161 Knowing $P(q)$ which is prescribed, one can determine the cloud fraction α_{cld} and

$$\alpha_{cld} = \int_{q_{sat}}^{+\infty} P(q) dq$$

162 where q_{sat} is the specific humidity at saturation. In the case of shallow convection, the
 163 subgrid water distribution is described by a bi-Gaussian distribution where the thermal
 164 plumes and their environment correspond to the small and the main modes of the dis-
 165 tribution, respectively (Hourdin et al., 2013, 2020; Madeleine et al., 2020). The param-
 166 eters required for the computation of this bi-Gaussian distribution are given by a ther-
 167 mal plume scheme. For a full description of the parameterization of clouds in LMDZ,
 168 the reader is referred to Madeleine et al. (2020).

Note that for

more ? ou plutôt
 equal nan ? à vérifier

This method can also be
 used to explore
 (quantify ?) the paramet-
 uncertainty of climate
 change projection.

Trop flou ; préciser
 le type d'erreur ;
 et je pense pas
 très bien la phrase.
 Pour moi c'est des truc
 différents :
 - exploration
 de l'erreur paramétri-
 - exploration de l'erreu
 paramétrique en ayant
 contraint BLABLA (=
 tes métriques)

independent on
 the location or
 the network

Due to a lack
 of physical
 modeling,
 the standard
 deviation is
 simply specified
 as $\sigma = \xi(p) q_t$
 where q_t is

to account for
 the fact that
 σ/q_t increases
 generally

which will not be considered
 here C'est vrai ?

cloud cover
 plutôt non ?

Even the
 in version

1) $q_t =$
 $\sigma =$

2) Thermig

3) Dans le cas
 qu'on nous
 inireve
 modèle
 plus simple

Rm

169 **2.1 Ice-supersaturation parameterization**

170 **2.1.1 The basic framework**

171 The parameterizations of clouds in LMDZ briefly introduced in the previous sec-
 172 tion are based on the assumption that water is always at thermodynamic equilibrium
 173 between the vapor and liquid phases or between the vapour and solid (ice) phases. How-
 174 ever, this assumption is not always met in the atmosphere, as some regions can be su-
 175 persaturated with respect to ice without being condensed (see Sect. 1). Our objective
 176 is that the model is able to create and maintain such ice supersaturated conditions in
 177 a realistic way so that ~~contrail cirrus~~ can be simulated and their effects and uncertain-
 178 ties be evaluated. ~~Given the coarse resolution of the atmospheric model, we consider that~~
 179 a given gridbox can be partitioned between an ice-subsaturated region (a thermodynamic
 180 equilibrium state with $q < q_{sat}$), an ISS region (a metastable thermodynamic state with
 181 $q > q_{sat}$), and a cloud fraction (in thermodynamic equilibrium state with total water
 182 $q > q_{sat}$). These three fractions are labelled *sub*, *ss* and *cld*, respectively. For this pur-
 183 pose, the parameterization needs to have a memory of the cloud fraction from one timestep
 184 to the next to track the fraction of the gridbox where condensation has occurred. The
 185 rationale for such a memory is that an ISS fraction can be converted into a cloudy frac-
 186 tion but the opposite is not true as the cloud can only sublimate in subsaturated condi-
 187 tions. The cloud cover α_{cld} is therefore used as semi-prognostic variable, by consid-
 188 ering it as an additional tracer ~~and~~ advected by the dynamical core, along with the hu-
 189 midity variables, but it does not formally follow a prognostic equation. We further as-
 190 sume, that cirrus clouds form only by homogeneous nucleation. ~~The treatment of cir-~~
 191 ~~rus cloud formation by heterogeneous nucleation would imply a representation of ice nu-~~
 192 ~~clei in the model, which is outside the scope of this study, that simply aims to show the~~
 193 ~~feasibility of introducing ice supersaturation in the model and tune the parameteriza-~~
 194 ~~tion against large-scale observables. Ice clouds can form through homogeneous freezing~~
 195 ~~when ice supersaturation exceeds a threshold $\gamma_{ss} q_{sat}$ that is a function of temperature~~
 196 ~~as specified by Koop et al. (2000) and Ren and Mackenzie (2005). The threshold of ice~~
 197 ~~supersaturation ratio, γ_{ss} , is expressed as:~~

198
$$\gamma_{ss} = \gamma_0 - T/T_\gamma$$
 (3)

199 where T is the temperature (in K) in the gridbox. The values of γ_0 and T_γ are 2.349 and
 200 259 K, respectively (Ren & Mackenzie, 2005). However, here, γ_0 and T_γ , denoted TGO
 201 and TG in Table 4, respectively, are considered as tuning parameters, because the data
 202 used to determine Equation 3 are subject to uncertainty. We characterize the three frac-
 203 tions of the gridbox through their respective cover, α_k (dimensionless) and their aver-
 204 age total water, q_k (kg kg^{-1}), expressed as a gridbox average. Thus the following con-
 205 servation equations apply:

205
$$\alpha_{sub} + \alpha_{ss} + \alpha_{cld} = 1$$

206 and

206
$$q_{sub} + q_{ss} + q_{cld} = q_t$$

207 where q_t is the total water in the gridbox.

208 **2.1.2 Subgrid water vapour distribution**

209 This parameterization fits well the pre-existing one in that it is also based on a sta-
 210 tistical treatment of water vapour at the subgrid scale (see Sect. 2). $P(q)$ is separated
 211 into three sub-PDFs P_{sub} , P_{ss} and P_{cld} that describe the total water in the *sub*, *ss*, *cld*
 regions, respectively. The three PDF are linked by the following relationship:

212
$$P(q) = \alpha_{sub} P_{sub}(q) + \alpha_{ss} P_{ss}(q) + \alpha_{cld} P_{cld}(q)$$
 (6)

213 The inclusion of P_{cld} is a new feature of this parametrization compared to the one in-
 troduced in Sect. 2. For q values above q_{sat} , P_{cld} is assumed to be proportional to P ,

$$P_{cld} = P \alpha_{cld} / \alpha_{cld}$$

ce serait
 pareil à 20 km
 non ?

Ne pas mélanger
 dans la même
 phase les
 motivations
 et la description
 du modèle

Ce veut
 dire quasi ?

Here, we

were fixed to

when developing the model

sof

so that

Je ne comprends pas

214 otherwise it is equal to 0 (see below). The lower bound of q for P_{cld} , denoted q^{vc} , cor-
 215 responds to the in-cloud water vapour. It is set equal to the specific humidity at satu-
 216 ration in the gridbox at the previous physical timestep and depends only on the tem-
 217 perature. It should be noted that the evaluation of q^{vc} is an approximation since it re-
 218 lies on the temperature of the gridbox at the previous timestep, while all the other quan-
 219 tities have been advected. This shortcoming is being addressed in the next version of the
 220 parameterization that is currently under development.

221 The coefficient of proportionality between P_{cld} and P for $q > q^{vc}$ is denoted N ,
 222 and derived from the following equation:

$$N = \alpha_{cld,adv} / \int_{q^{vc}}^{+\infty} P(q) dq \quad (7)$$

223 As q values can exceed saturation in both the ISS and the cloudy fractions, N is in the
 224 range 0 to 1 by construction. Specifically, $N \in]0, 1[$ corresponds to situations where the
 225 three fractions coexist in the gridbox, $N = 0$ corresponds to situations where only sub-
 226 saturated region and ISS fractions coexist, while $N = 1$ corresponds to situations where
 227 only subsaturated region and cloudy fractions coexist. Knowing N and q^{vc} , the normalised
 228 PDFs of P_{sub} , P_{ss} and P_{cld} are determined as follows:

$$P_{sub}(q) = \begin{cases} P(q)/\alpha_{sub} & \text{if } q < q^{vc} \\ 0 & \text{otherwise} \end{cases} \quad (8)$$

$$P_{cld}(q) = \begin{cases} 0 & \text{if } q < q^{vc} \\ N P(q)/\alpha_{cld,adv} & \text{otherwise} \end{cases} \quad (9)$$

$$P_{ss}(q) = \begin{cases} 0 & \text{if } q < q^{vc} \\ (1 - N) P(q)/\alpha_{ss} & \text{otherwise} \end{cases} \quad (10)$$

229 where $\alpha_{clr} = \int_0^{q^{vc}} P(q) dq$ and $\alpha_{ss} = 1 - \alpha_{clr} - \alpha_{cld,adv}$ at this stage.

230 P_{cld} and P_{ss} are diagnosed at each timestep, and are proportional. When a cloud
 231 form above $\gamma_{ss} q_{sat}$, the distributions are not proportional anymore. When they are re-
 232 diagnosed in the following timestep and are proportional one to another, there is there-
 233 fore a non-physical humidity flux from high humidities to low humidities in the cloud,
 234 and the other way around in the ISSR. This leads to an overestimation of the cloud for-
 235 mation. To address this limitation, it is assumed that a larger part of the region with
 236 $q < \gamma_{ss} q_{sat}$ is covered by clouds. For that purpose, the value of the proportionality co-
 237 efficient N is increased to $N_2 = \Phi_N N$ for $q > \gamma_{ss} q^{vc}$ and to $N_1 = \Phi_N N$ for $q^{vc} <$
 238 $q < \gamma_{ss} q^{vc}$, where Φ_N is a tuning parameter that can take values in the range 1 to 2.
 239 It is worth noting that P_{sub} in the subsaturated region is determined by the knowledge
 240 of q^{vc} and $P(q)$. The characteristics of P_{sub} are imposed by the pre-existing parameter-
 241 ization whereas that of the cloudy fraction is imposed by the new parameterization. This
 242 sometimes creates situations where $\alpha_{cld,adv} + \alpha_{clr} > 1$, leading to a loss of memory as
 243 we impose $\alpha_{cld,adv} + \alpha_{clr} \leq 1$. To avoid losing the memory, $P(q)$ has been slightly mod-
 244 ified so that when $\alpha_{cld,0}$ is high, the PDF is not constraining the subsaturated region to
 245 be large. In the former parameterization, the PDF was very unlikely to diagnose a large
 246 cloud fraction, whereas this is often the case in the new one. The function $\xi(p)$ for the
 247 new parameterization is then computed as follows:

$$\xi(p, \alpha_{cld,adv}) = \frac{\xi_{old} dp}{1 + \beta \cdot \alpha_{cld,adv}} \quad (11)$$

248 where β is a tuning parameter whose value is between 0 and 5.

Table 1. List of ice saturation parameterisation parameters. For each parameter, the range of values, the default or First Guess (FG) value and the physical process controlled are indicated. The names of the parameters as used in the tuning process are given in brackets.

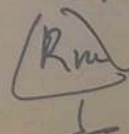
Name	Unit	Range	FG value	Controlled processes
T_γ (TG)	K	[249, 269]	259	Saturation rate for homogeneous nucleation
γ_0 (TG0)	-	[2.3, 2.4]	2.349	Saturation rate for homogeneous nucleation
N (TN)	-	[1, 2]	1.1	Ratio between the ISSR and in-cloud water distributions PDFs
ratqs (RQST)	-	[1, 5]	3.0	Width of the sub-grid relative humidity PDF
ξ (KHI)	-	[1, 10]	1.1	Boundary size between ISSR, clear sky and cloudy region
lturb (LTURB)	m	[25, 200]	50.0	Turbulent mixing length around the cloud

2.1.3 Sublimation and condensation

In this work, the treatment of sublimation and condensation are not diagnosed from prognostic equations, but from the distribution $P(q)$. Ice clouds sublimate when q_{cld} becomes smaller than q_{sat} . The condensed excess moisture is the fraction that exceeds the nucleation threshold $\gamma_{ss} q_{sat}$, according to the PDF of P_{ss} . These two processes are computed using the semi-prognostic value of $\alpha_{cld,adv}$. The variations of α_{cld} due to sublimation, $(\Delta\alpha_{cld})_{sub}$, and condensation, $(\Delta\alpha_{cld})_{cond}$, are computed first. These tendencies are added to $\alpha_{cld,adv}$ to obtain α_{cld} for the current timestep.

2.1.4 Turbulence

Small-scale turbulence may mix the cloudy region in the gridbox with the subsaturated and ISS regions. The turbulence is parameterized using a characteristic velocity, v_{turb} , and a characteristic length, l_{turb} . The v_{turb} variable is determined as an approximation of the diagnosed Turbulent Kinetic Energy (TKE) and l_{turb} is a tuning parameter with a typical value of the order of ten to a hundred metres but we used a default value of 50 m. It is also assumed that cirrus clouds have the shape of a prolate spheroid shape (Fig. 1). This approximation has the advantage of being relevant to model both natural cirrus and contrails. It is also assumed that all the mass that is transferred from the cloud to the environment, or vice versa, occurs within an area around the cloud delimited by a length $L = \min(v_{turb}\Delta t, l_{turb})$. In the environment, this area is that between the boundary (distance R from the centre) and that at distance $R+L$ from the centre (Fig. 1). In the cloud, it is the area between the boundary and that at distance $R-L$ from the centre. It is also assumed that these two areas are well mixed by turbulence. The volume of the cloud environment, V_{env} , is the sum of the volumes of the subsaturated region, V_{sub} , and ISS, V_{ss} , which can be expressed through the introduction of a parameter σ , such that $V_{ss} = \sigma V_{env}$ and $V_{sub} = (1-\sigma) V_{env}$. However σ may deviate from $\alpha_{ss}/(\alpha_{ss} + \alpha_{sub})$ because the three fractions are distributed homogeneously in the gridbox. Thus another tunable parameter χ is introduced so that $\sigma = \alpha_{ss}/(\chi\alpha_{sub} + \alpha_{ss})$. This formulation of σ accounts for the fact that there is a higher probability that the cloud and ISS fractions are in contact (which implies $\chi > 1$). In the ISSR, the diffusion of crystals leads to further condensation of ice so that part of the ISSR becomes cloud, with corresponding changes in their fraction and total water content. The equations of the parameterization of turbulence and the full description of the parameterization are provided in detail in Borella et al. (2021). It should be noted that this parameterisation in LMDZ is only applied for temperatures below -30°C , which corresponds to the temperature at altitudes in the upper troposphere where contrails can form.

Env (env)


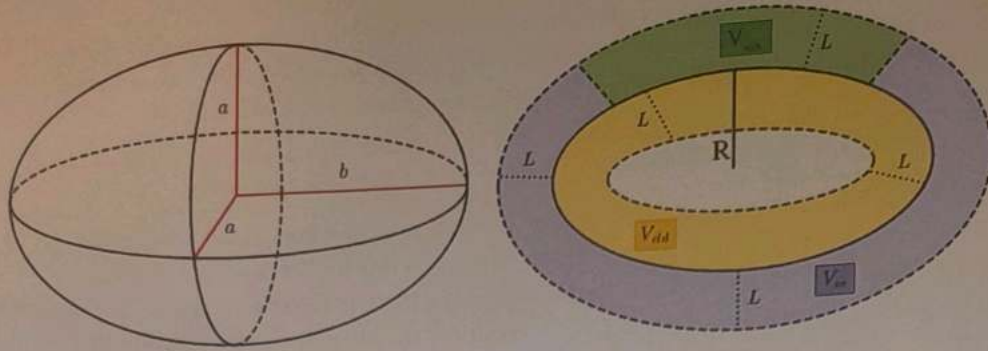


Figure 1. Left panel: Prolate spheroid illustrating our assumption on the shape of clouds. The spheroid has semi-axes a and b . This assumption allows us to take into account the wispy nature of cirrus clouds and the very high surface-to-volume ratio of contrails, but not the fact that the stratified atmosphere at this altitude limits the vertical extension of these clouds. Right panel: Schematic distribution of the quantities V_{cld} , V_{sub} and V_{env} in the cloud boundary layer. L is the width of the turbulent mixing zone while R is the distance from the centre of the cloud to the border of the environment around the cloud.

On met l'erreur d'incertitude dans la "tolérance à l'erreur"

3 Experimental Setup

3.1 History matching and iterative refocusing

The history matching with iterative refocusing is based on the idea of i) running a perturbed physics ensemble (PPE) of simulations with the climate model in a pre-defined parameter space, ii) using the output to train statistical emulators that predict the metrics of interest, and then iii) using the emulator to rule out regions of parameter space for which its predictions are "too far" from observations (D. B. Williamson et al., 2017). The process is iterative: at the end of each iteration, a new PPE is run in order to improve the quality of the emulator and refine the search for potentially good model configuration, but only in a relevant subspace, i.e. outside the region of space already ruled out. This introduces the notion of the relevant parameter space, which evolves during the iterative process. The method rigorously takes into account the various sources of uncertainties (from both the emulator and the observations) and a tolerance level in order to avoid over-tuning the climate model. It is implemented in different steps, as described in the following subsections.

3.1.1 Selection of the targeted metrics

The first step consists of defining the targeted metrics (f), which are scalars that are used to quantify the behaviour of a simulation. For each metric, we set a reference value (r_f) and an associated uncertainty ($\sigma_{r,f}$). The different metrics used are described in Section 3.3 and their reference values are provided in Tables 2 and 3.

C'est pas une associated uncertainty, c'est une tolérance à l'erreur > l'incertitude quantifiée (ici j'imagine que c'est l'incertitude de tes obs et éventuellement liée à ta configuration). En toute logique ce serait mieux qu'elle s'appelle pas sigma

3.1.2 Identification of the free parameters

The free parameters to be tuned must be selected and a range of acceptable values defined for each of them, as well as their initial input space (I), need to be defined. The chosen parameters must be compatible with the target metrics. In this work, a set of 23 parameters, presented in Table 4, are selected as candidates for the tuning. Any combination of these parameters is called a vector and denoted λ in the following.

ce n'est pas ce que j'ai compris ce que tu voulais dire
pourquoi candidates?

in toute rigueur
pour éviter
re-tuning /
refitting
indrait par
force connaître
leur structurelle
modèle ; ce que
est en pratique
mais le cas avec
des de climat. Mais
est-être un peu pointu
sur une intro de partie

proposition : The method required that the various sources of uncertainties be quantified in order to avoid over-tune the model. (eventuellement :) An estimation of the uncertainty of the prediction of the emulators is also accounted for in the method.

c'est ça. C'est pour ça que on a décidé de tout mettre dans "tolérance à l'erreur"

Targets
Contra de l'objectif (A)
à priori range ou non incertitude
NRCY parameter space pour être plus précis ?
1. Je suis pas 100% d'acc avec cette phrase -> il n'y pas que les err d'emulateurs et d'observations qu'il faut prendre en compte mais bien TOUTES les sources d'incertitudes entre ton setup experimental et tes références, ce qui peut inclure beaucoup de choses comme la variabilité interne du modèle, la sensibilité à tes forçages etc. Je trouve ça dommage de laisser entendre qu'il n'y aurait en toute généralité que ces deux sources d'erreurs à quantifier

3.1.3 Experimental design

The experimental design consists of drawing a sample of values (λ) of parameters from the initial parameter space. For each of these λ (here 300), a simulation is run with the climate model, the output of which are used to calculate the metrics that serve as a training set for the statistical emulators. To ensure optimal sampling of the input parameter space, a Latin hypercube method is used (D. Williamson et al., 2015).

3.1.4 Building of the surrogate models

An emulator based on Gaussian Processes (GP) is then built for each metric. The emulator gives a statistical estimate of the corresponding metric value at any point of the parameter space (T for the first wave and the successive Not-Ruled-Out-Yet (NROY) space for subsequent waves), providing both the expectation ($E[f(\lambda)]$) and the variance ($Var[f(\lambda)]$) of the uncertainty associated with the statistical emulator prediction of each metric.

3.1.5 History matching

The history matching aims to identify the subspace of free parameter values compatible with the reference data, under the constraints (metrics) chosen in step 1 (Section 3.1.1). For a vector λ of parameters, a measure noted $I_f(\lambda)$ is introduced to quantify its implausibility:

that matches a set of metrics, given their tolerance to error

$$I_f(\lambda) = \frac{|r_f - E[f(\lambda)]|}{\sqrt{\sigma_{r,f}^2 + \sigma_{t,f}^2 + Var[f(\lambda)]}} \quad (12)$$

where r_f and $\sigma_{r,f}$ are the target reference value for the metric f and the associated uncertainty (whose distribution is assumed to be Gaussian), respectively. $Var[f(\lambda)]$ is the variance of the uncertainty associated with the statistical emulator prediction and $\sigma_{t,f}$ is the structural error (also assumed to follow a Gaussian distribution) of the climate model for the metric f (D. Williamson et al., 2015). This structural error can be difficult to estimate and D. Williamson et al. (2015) suggest that it should be interpreted as a tolerance to error. We have considered a tolerance to error of 0.1 (i.e., 10 % for the RHi and the high-level cloud metrics. A tolerance to error of 10 % is considered for the IWP metrics (i.e., 10 % of the value of each metric) given the large uncertainties associated with them.

Oui, mais par contre la tolérance à l'erreur regroupe cette "structural model error" et les autres incertitudes que tu as pu quantifier = celle de l'obs ici (mais pas celle de la prédiction de l'émulateur)

The NROY space is defined from the implausibility in a multi-metric framework as follows:

$$NROY = \bigcap_f \{ \lambda \mid I_f(\lambda) < T \} \quad (13)$$

where T a threshold to be defined. Here it is set to 3 according to the rule of Pukelsheim (1994) which indicates that 95% of any unimodal Gaussian distribution lies within ± 3 standard deviations around its mean value. This choice implies that there is a 5% risk of discarding a plausible value from the NROY space.

C'est quoi le f de NROYf space ?

3.1.6 Iterative Refocusing

The implausibility $I_f(\lambda)$ for a vector (λ) of parameters can be small either because the simulated metric is close to its reference, or because the emulator uncertainty at λ is high. Iterative Refocusing aims to reduce the uncertainty due to the emulator. Consequently, several iterations (or waves) of steps 3–5 (Sections 3.1.3, 3.1.4 and 3.1.5) are performed, using for the wave n the NROY issued from the wave $n-1$ ($NROY^{n-1}$). The process is stopped when the NROY space is stable because the emulator uncertainty is sufficiently reduced so that the other uncertainty types dominate the implausibility. In

(so that it is plausible and not ruled out yet)

Je trouve qu'il manque l'information que l'incertitude de la prédiction de l'émulateur réduit au cours des itérations parce que les emulateurs sont construits dans des espaces où ils sont + échantillonnées (tu as le même nombre de "training data set" = 300 pour un espace de plus en plus petit au fur et à mesure des itérations)

Ce n'est malheureusement pas toujours le cas. Tu peux ne plus diminuer ton NROY au cours des itérations et avoir certaines métriques qui gardent une incertitudes des prédictions de l'émulateur du même ordre de grandeur que ta tolérance à l'erreur (voir des fois beaucoup plus grande). Je ne sais pas ce que ça donne dans ton expérience.

In peu plus généralement sur 3.1.5 et 3.1.6 : tu dis au début de 3.1.5 que l'objectif de l'history mathing c'est de trouver les sous-espace des paramètres acceptables ; mais en fait cet objectif c'est celui de toute la méthode. Je pense que cette phrase devrait apparaître dans ton premier paragraphe du coup

J n'as pas introduit 1D avant, c'est peut être pas très compréhensible comme ça. D'ailleurs je sais pas si 1D/3D c'est bien compréhensible
 n'utilise plus SCM vs global.
 proposition: In this study, we follow the approach of Hourdin et al 2021 and start by carrying out 9 successive waves with (the same) metrics
 single column (SCM) test cases. We then carry out 3 waves with additional metrics evaluated on global simulations

352 this study, we followed Hourdin et al. (2021) by carrying out 9 tuning successive waves
 353 of the 1D version of the model, followed by 3 waves combining the 1D and 3D versions
 354 of the model. It is the result of the last wave, i.e. the twelfth, that is essentially discussed
 355 in what follows.

3.2 Simulations and forcing

th the first year
 considered as
 in-up (?)

356 Simulations with the 3D and 1D (single column) versions of LMDZ are carried out
 357 in this study. The 3D simulations are forced by the seasonal cycle of SST and Sea Ice
 358 Cover (SIC) following the Atmospheric Model Intercomparison Project (AMIP) proto-
 359 col. The duration of 3D simulations is 2 years. LMDZ turns out to have a temperature
 360 bias in the upper troposphere and lower stratosphere (Fig. 2), which can impact the fre-
 361 quency of occurrence of ISSRs since homogeneous nucleation is controlled by temper-
 362 ature (Sections 2 and 2.1). This cold bias is observed both with the pre-existing and the
 363 new parameterization, which means it is likely a model structural deficiency that is in-
 364 dependent of the representation of ISSRs. As our objective is to show the feasibility of
 365 tuning the ISS parameterization, reducing this longstanding temperature bias by new
 366 model developments would involve complex research beyond the scope of this study, in-
 367 stead we reduce using temperature nudging. To this effect, we first performed a nudged
 368 simulation, whereby the LMDZ meridional (u) and zonal (v) wind and the temperature
 369 (T) fields are relaxed toward those of the fifth generation of the European Centre for Medium-
 370 Range Weather Forecasts atmospheric reanalysis (ERA5) as formalized in the following
 371 equation:
 372

Rentrait une section à part. C'est pas qu'on a à aller
 mettre de la correction
 de biais dans un exercice
 de tuning. Aïen le justifier.

$$\frac{\partial X}{\partial t} = F(X) + \frac{X^a - X}{\tau}$$

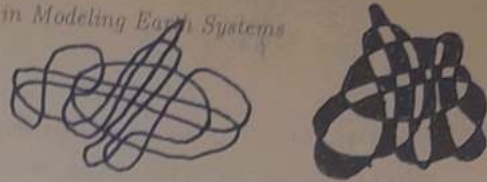
373 where F is the operator describing the dynamical and physical processes that determine
 374 the unconstrained evolution of X , X^a is the 6-hourly reanalysis fields from ERA5, in-
 375 terpolated to the model grid and model timestep, and τ is a relaxation time constant
 376 (Coindreau et al., 2007; Krinner et al., 2020), set to 1 day in this study. The nudging
 377 is not applied in the atmospheric boundary layer. The nudged simulation is carried out
 378 for 10 years and the error terms $(X^a - X)/\tau$ are archived. The 10-year (i.e., climato-
 379 logical) monthly-averages of $(X^a - X)/\tau$ are then computed and used to correct the model
 380 online in all the remaining simulations of this study. More details on this bias correc-
 381 tion method, their benefits and their limitations can be found in Krinner et al. (2020).
 382 We tested the bias correction method using the averaged relaxation terms of u , v and
 383 T and u and v only. The former approach is retained for this study because it allows a
 384 better correction of the LMDZ bias in temperature in the UTLS. Fig. 2 illustrates the
 385 remaining error for the North Atlantic and Europe at 250 and 200 hPa. The error that
 386 persists is greater at 200 hPa in Europe.

387 Single Column Model (SCM or 1D) simulations are performed for four observational
 388 case studies for which Large Eddy Simulations (LES) have been developed. The first case
 389 is an almost cloud-free convective boundary layer case observed on June 14, 2002 over
 390 the Southern Great Plain during the International H₂O Project (IHOP) campaign (Couvreur
 391 et al., 2005). The second case deals with the diurnal cycle of shallow convection over land
 392 observed on June 21, 1997, with fairly well-developed cumulus at the Atmospheric Ra-
 393 diation Measurement site in Oklahoma (Brown et al., 2002). The third case is about a
 394 rain cumulus over the ocean (VanZanten et al., 2011). The fourth case is a composite
 395 transition case of stratocumulus to cumulus clouds, as described by Sandu and Stevens
 396 (2011). These case studies are named IHOP/REF, ARMCU/REF, RICO and SANDU,
 397 respectively. The different SCM simulations carried out are not nudged and are described
 398 in details with those of the associated LES in Couvreur et al. (2021) and Hourdin et al.
 399 (2021).

En fin



Pk ?



3.3 Tuning metrics and references

3.3.1 SCM Metrics

The SCM metrics used are the mixed layer potential temperature and humidity, the average cloud height and the height of the maximum cloud fraction. LES are used as reference. These metrics and the LES simulations are described in details in Couvreux et al. (2021) and Hourdin et al. (2021).

Eventuellement expliquer en deux mots l'intérêt de faire ça = enlever les vecteurs de paramètre qui font de la "mauvaise" convection peu profonde ?

3.3.2 Metrics of radiative fluxes and precipitation

The radiative metrics considered in this work are those used in Hourdin et al. (2021). They include metrics of global net radiation (i.e. the imbalance between shortwave (SW) and longwave (LW) and global top-of-atmosphere (TOA) SW upward radiation). As the SW downward radiation is imposed on the model, the global outgoing LW radiation will be constrained automatically by the constraints on the SW and total radiation (Hourdin et al., 2021). Metrics also consider regional averages of the TOA outgoing LW and SW radiation, distinguishing convective, subsidence and intermediate regimes in the tropics and a contrast in latitude between the roaring forties and tropical oceans targeting a circum-Antarctic warm bias in coupled ocean-atmosphere simulations. A specific metric is dedicated to the SW contrast between Eastern Tropical Oceans and the rest of the tropics following (Hourdin et al., 2015). The CERES-EBAF L3b observational dataset (Loeb et al., 2009) is used as reference. The locations where these metrics are computed are indicated in Hourdin et al. (2021) and their values and associated uncertainties are presented in Table 2.

Dire que ces métriques sont le moyen choisi actuellement pour régler LMDZ afin qu'il simule un bon climat ? Ou qu'on considère que ces métriques définissent ce qu'est bon climat pour l'atmosphère ?

Oui : je pense que ça va venir de cycles qui dirait. Ça revient ce qu'on essaie de faire :

The rainfall metrics used are the global mean rainfall of daily rainfall larger than 50 mm ($PR > 50$), the mean annual rainfall over a box over Western Africa used for the African Monsoon Multi-disciplinary Analysis (AMMA) campaign, and finally an estimate of the intra-seasonal variability over the ocean in the region of the Madden-Julian Oscillation (MJO), computed from the daily rainfall as the standard deviation of the 20-day running average minus the 120-day running average using the Global Precipitation Climatology Project (GPCP, Huffman et al., 2001) daily precipitation data as reference. The values of these metrics and the associated uncertainties are provided in Table 2.

3.3.3 RHi metrics

In addition to the metrics used in Hourdin et al. (2021), we selected a range of metrics that relate more specifically to our ISS parameterization. These metrics include the 80th (P1) and 95th (P2) percentiles of the RHi distributions at 250 and 200 hPa above the North Atlantic (NA hereafter) and Europe (EU hereafter) (see Table 3). Data used as reference are from the Measurement of Ozone and water vapour on Airbus airCRAFT In-service (MOZAIC) programme (Marengo et al., 1998) over the period 1995-2014 and from the In-service Aircraft for a Global Observing System (IAGOS) programme (Petzold et al., 2015) over the period 2011-2023. For the sake of simplicity, we refer to these two databases as IAGOS in the following. These data are measured every four seconds with uncertainties ranging from 2% to 8% (5% on average) at the cruising altitude (Smit et al., 2014; Petzold et al., 2020). Due to the inhomogeneous sampling in time (e.g., more measurements in summer) and space (e.g., more measurement at 250 hPa than 200 hPa in the North Atlantic) by the IAGOS and MOZAIC aircraft, some atmospheric conditions are potentially oversampled and this may lead to biases in the long-term RHi distribution at the regional scale (Sanogo et al., 2024). This temporal and spatial sampling uncertainty is difficult to characterize (Sanogo et al., 2024). To partly take this into account, we consider a total uncertainty of 8%. A moving average of 17 minutes (corresponding to ~255 km at cruising speed) is also applied to these RHi observations to make them comparable to the gridbox average of RHi in LMDZ. It should be noted that IA-

= Revenir le modèle avec la nouvelle pour exactement comme on fait au ce moment pour LMDZ en ajoutant des métriques spécifiques.